# Synthesis, X-ray and Quantum Chemical Characterizations Studies on (*E*)-2-Bromo-4-chloro-6-[(4-chloro-2,5-dimethoxyphenylimino)methyl]phenol Compound

Cem Cüneyt ERSANLI[1,*], Başak KOŞAR KIRCA[2], Çiğdem ALBAYRAK KAŞTAŞ[3]

[1] *Department of Physics,  Faculty of Art and Science, Sinop University, 57000, Sinop, Turkey.*

[2] *Division of Science Education, Faculty of Education, Sinop University, 57100 Sinop, Turkey.*

[3] *Department of Chemistry,  Faculty of Art and Science, Sinop University, 57000, Sinop, Turkey.*

**Abstract**

In the present work, new Schiff-base derivative of (*E*)-2-bromo-4-chloro-6-[(4-chloro-2,5-dimethoxyphenylimino)methyl]phenol, formula sum is given by $C_{15}H_{12}BrCl_2NO_3$ (**I**), has been synthesized and characterized by single-crystal X-ray diffraction and density functional theory (DFT) molecular orbital calculations. The title compound displays O-H…N intramolecular, weak C-H…O, C-H…Cl intermolecular and a weak π-π stacking interactions which influence crystal packing. The experimental results were compared to the theoretical ones, obtained at DFT level. Theoretical electronic structure calculations of the B3LYP/6-311G(d,p) level were performed to optimize the molecular geometry. The values of the total dipol moment (*μ*), linear polarizability (*α*) and the first hyperpolarizability (*β*) of the investigated compound were computed using B3LYP/6-311G(d,p) calculations. The energetic behaviors of (**I**) in different solvents were examined by using time-dependent DFT method and applying the polarizable continuum model. Mulliken population analysis (MPA), frontier molecular orbitals (FMOs), molecular electrostatic potential and thermodynamic properties were also calculated.

## 1. INTRODUCTION

Schiff-bases which contain the imino group (–RC=N–) are formed by condensing a primary amine with an activated carbonyl group. In search of new drugs, Schiff-bases have been evaluated for a range of bioactivities such as antimicrobial, antialzheimer, anticancer, antiglycation, antileishmanial, antituberculosis, anti-convulsant, anti-inflammatory, antioxidant, antiviral, urease inhibition, pesticidal activity, *etc*. [1-3].These compounds are used for industrial purposes. For example; pigments, catalysts, intermediates in organic synthesis and as polymer stabilizers [4]. Schiff-bases between molecules have therapeutic potential for the treatment of various human diseases. The photochemistry of the Schiff-base molecules influence these properties greatly, and also these molecules are highly affected by the crystal structure. Therefore, the study of crystal packing and the intermolecular interactions in the crystal structures of various Schiff-bases can lead to valuable data for the design and synthesis of new materials. In this paper, we wish to report the synthesis, characterization, crystal structure and theoretical studies of the newly synthesized Schiff-base compound (*E*)-2-bromo-4-chloro-6-[(4-chloro-2,5-dimethoxy-phenylimino)methyl]phenol, (**I**).

## 2. EXPERIMENTAL

### 2.1. Synthesis and Crystallization

The compound (*E*)-2-bromo-4-chloro-6-[(4-chloro-2,5-dimethoxyphenylimino)methyl]phenol (Figure 1) was prepared by stirring under reflux a mixture of 3-bromo-5-chloro-2-hydroxybenzaldehyde (0.46 g,

---

1.95 mmol) in ethanol (20 ml) and 4-chloro-2,5-dimethoxyaniline (0.37 g, 1.95 mmol) in ethanol (20 ml). The crystals suitable for X-ray analysis were obtained from ethanol (yield; 72%, m.p.; 172-173 $^{\circ}$C).
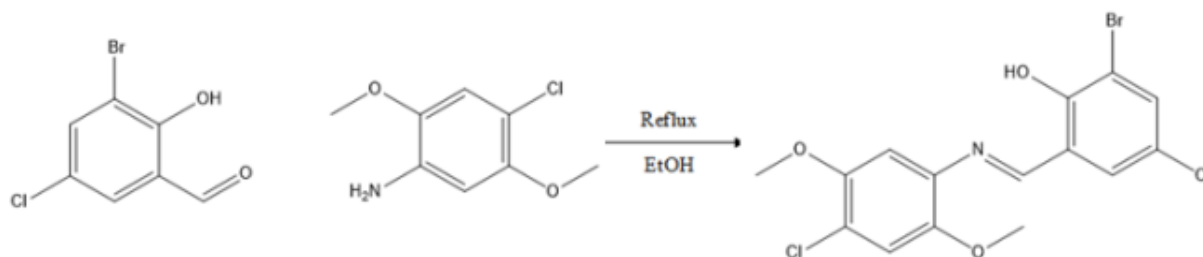


**Figure 1.** *Synthesis of (E)-2-bromo-4-chloro-6-[(4-chloro-2,5-dimethoxyphenylimino)methyl]phenol*

## 2.2. X-ray Diffraction Analysis

A yellow coloured prismatic single crystal of dimensions 0.12x0.14x0.19 mm$^3$ of (**I**) was chosen for an X-ray diffraction study. The crystallographic data were collected at 293 K on a Bruker APEX-II CCD diffractometer [5], using graphite monochromatized MoK$_\alpha$ ($\lambda$=0.71073Å). Data reduction was performed using the Bruker Saint. The structure was solved by direct methods and refined by full-matrix least squares method on $F^2$ using SHELXS [6] and SHELXL [7] programs. Hydrogen atoms except hydrogen bonded O1 were placed in geometrically idealized positions and refined as riding atoms with $U_{iso}$=1.5$U_{eq}$ (C) for methyl H atoms and 1.2$U_{eq}$ (C) for the remaining H atoms. WinGX [8], ORTEP-III for Windows [8] and Mercury [9] software packages were used for molecular drawing and other materials. Details of crystal data, data collection, structure solutions and refinements were given in Table 1.

**Table 1.** *Crystal data and structure refinement parameters for (**I**)*

| | |
|---|---|
| CCDC Deposit No | CCDC: 1532550 |
| Empirical Formula | $C_{15}H_{12}BrCl_2NO_3$ |
| $M_r$ | 405.07 |
| Crystal system, space group | Monoclinic, C2/c |
| Temperature (K) | 293 |
| $a$, $b$, $c$ (Å) | 26.2280(16), 7.2214(4), 16.7975(11) |
| $\beta$ (°) | 99.290(2) |
| $V$ (Å$^3$) | 3139.8(3) |
| $Z$ | 8 |
| $F$(000) | 1616 |
| $D_x$ (Mg m$^{-3}$) | 1.714 |
| Radiation type | MoK$\alpha$ |
| No. of reflections for cell measurement | 9959 |
| $\theta$ range (°) for cell measurement | 2.93-26.00 |
| $\mu$ (mm$^{-1}$) | 2.969 |
| Crystal shape | Prism |
| Colour | Yellow |
| Crystal size (mm) | 0.12 × 0.14 × 0.19 |

| Scan method | $\varphi$ and $\omega$ scans |
|---|---|
| $T_{min}$, $T_{max}$ | 0.4485, 0.7457 |
| No. of measured, independent and observed [$I > 2\sigma(I)$] reflections | 36504, 3086, 2742 |
| $R_{int}$ | 0.0385 |
| Range of $h$, $k$, $l$ | $h = -32\rightarrow32$, $k = -8\rightarrow8$, $l = -20\rightarrow20$ |
| Refinement on | $F^2$ |
| $R[F^2>2\sigma(F^2)]$, $wR(F^2)$, $S$ | 0.0310, 0.0732, 1.135 |
| No. of parameters | 207 |
| Weighting scheme | $w = 1/[\sigma^2(F_o^2) + (0.0281P)^2 + 5.0193P]$ where $P = (F_o^2 + 2F_c^2)/3$ |
| $(\Delta/\sigma)_{max}$ | $< 0.001$ |
| $\Delta\rho_{max}$, $\Delta\rho_{min}$ (e Å$^{-3}$) | 0.346, -0.468 |

### 2.3. Computational Details

All theoretical calculations were performed using Gaussian03W program [10] and Gauss-View4.1.2 molecular visualization program package [11] on the personal computer. The Becke three parameter hybrid exchange [12,13] and the Lee-Yang-Parr correlation functionals [14] (B3LYP) were used. Geometry optimization of the studied molecule was carried out with the DFT method using 6-311G(d,p) basis set. Firstly; the calculations were started with the crystallographically obtained geometrical data of (**I**). Secondly, in order to show non-linear optic (NLO) activity and reactive sites of the molecule, $\mu$, $\alpha$ and $\beta$ from the Gaussian output were previously explained in detail. Thirdly, some properties such as total energy, the highest occupied molecular orbital (HOMO) and the lowest unoccupied molecular orbital (LUMO) energies, the global hardness ($\eta$), electronegativity ($\chi$), and softness ($S$) for enol-imine form of (**I**) were obtained at the B3LYP/6-311G(d,p) level in gas phase, in order to investigate the tautomeric stability. These properties were also examined for (**I**) in various solvent media (including benzene, chlorobenzene, ethanol, methanol and water) at the B3LYP/6-311G(d,p) level using the Polarizable Continuum Model (PCM) method [15]. Finally, MPA, FMOs, MEP and thermodynamic functions of (**I**) were obtained at the same method in gas phase.

## 3. RESULTS AND DISCUSSIONS

### 3.1. Crystallographic Studies

The title compound is crystallized in the monoclinic space group C2/c. The molecular structure of (**I**) with the atom numbering scheme is given in Figure 2. The selected bond distances and bond angles for the compound (**I**) are shown in Table 2. All bonds distances and angles are normal, and are in good agreement with those reported in similar Schiff-base compounds [16-19]. The N1=C9 bond length of 1.275(3) Å in (**I**) conforms to the value for a double bond, while the N1-C1 bond length of 1.406(3) Å in (**I**) conforms to the value for a single bond, like in similar Schiff-base compounds [20-22]. The C=N double bond has an *E* configuration. X-ray crystallography analysis of the compound reveals that the C15-O1 [1.331(3) Å] bond length indicates a single bond character, whereas the C9-N1 [1.275(3) Å] bond length indicates a double bond character. Hence, the prototropic hydrogen atom (H1) is located on the atom O1, thus showing a preference for the phenol-imine tautomer in the solid state. In the structure, O-C bond lengths are in the range of 1.331(3)-1.433(3) Å. C-C, C-Br and C-Cl bond lengths are in the expected range.
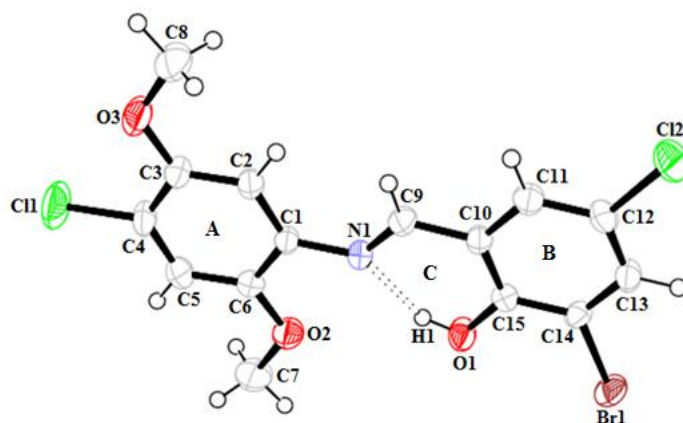
***Figure 2.*** *ORTEP-III of (**I**) with thermal ellipsoids drawn at 50% probability*

The conformation of the molecule can be described by the dihedral angle between the aromatic rings. This torsion defines the conformation of the chain bridging the two phenyl rings in (**I**) value C1-N1-C9-C10=178.9(2)°. According to Moustakali-Mavridis *et al.* [23], photochromic and thermochromic properties are associated with the molecular planarity in Schiff-bases. The dihedral angle between A (C1/C6) and B (C10/C15) rings showing the planarity of (I) is 2.28(8)° and this planarity may lead to a thermochromic feature. *o*-Hydroxysalicylidene systems have common properties, such as the type of a strong intramolecular hydrogen bond. There is a strong intramolecular O-H⋯N hydrogen bond between atoms N1 and O1 of the title molecule. The intramolecular O1-H1⋯N1 hydrogen bond leads to the formation of an almost planar six-membered ring C (N1/C9/C10/C15/O1/ H1). Then, this bond is oriented, in this ring C, with respect to rings A and B at dihedral angles of A/C=2.92(9)° and B/C=0.94(9)°. So it is coplanar with adjacent ring B and generates an *S*(6) ring motif (Figure 2).

***Table 2.*** *Comparison of X-ray parameters and DFT parameters of (I)*

| Bond length (Å) | X-ray | DFT |
|---|---|---|
| Br1-C14 | 1.886(2) | 1.8857 |
| Cl1-C4 | 1.737(2) | 1.7369 |
| Cl2-C12 | 1.742(2) | 1.7416 |
| N1-C1 | 1.406(3) | 1.4064 |
| N1-C9 | 1.275(3) | 1.2754 |
| O1-C15 | 1.331(3) | 1.3305 |
| O2-C6 | 1.362(3) | 1.3618 |
| O2-C7 | 1.433(3) | 1.4331 |
| O3-C3 | 1.362(3) | 1.3614 |
| O3-C8 | 1.427(4) | 1.4271 |
| C10-C11 | 1.398(3) | 1.3975 |
| C10-C15 | 1.412(3) | 1.4124 |
| **Bond angle (°)** | | |
| N1-C9-C10 | 121.0(2) | 120.9671 |
| O1-C15-C10 | 121.8(2) | 121.7643 |
| O1-C15-C14 | 120.2(2) | 120.1843 |
| O2-C6-C1 | 116.3(2) | 116.2658 |
| O2-C6-C5 | 124.5(2) | 124.5316 |
| O3-C3-C4 | 117.8(2) | 117.7953 |
| O3-C3-C2 | 124.4(2) | 124.2195 |
| C2-C1-N1 | 124.0(2) | 123.9765 |
| C6-C1-N1 | 116.4(2) | 116.3845 |

| C9-N1-C1 | 123.5(2) | 123.5127 |
|---|---|---|
| C13-C14-Br1 | 119.1(2) | 119.0811 |
| C15-C14-Br1 | 119.1(2) | 119.1483 |
| **Torsion angle (°)** | | |
| N1-C1-C6-O2 | -1.2(3) | -1.1822 |
| N1-C1-C2-C3 | -179.5(2) | -179.4829 |
| N1-C1-C6-C5 | 179.0(2) | 179.0402 |
| C1-N1-C9-C10 | 178.9(2) | 178.9150 |
| C2-C1-C6-O2 | 179.0(2) | 178.9887 |
| C9-N1-C1-C2 | 3.9(4) | 3.8882 |
| C9-N1-C1-C6 | -175.9(2) | -175.9327 |
| O1-C15-C14-Br1 | -1.9(3) | -1.8935 |
| Br1-C14-C13-C12 | -178.4(2) | -178.4134 |

The intermolecular C7-H7A⋯O1 and C-H⋯Cl and π…π interactions are important in the crystal packing of (**I**) to form a three-dimensional network. This slipped π…π interaction occurs between phenyl rings, where Cg(1)⋯Cg(2)$^i$=3.6688(14) Å (*i*: -*x*, 2-*y*, -*z*); Cg(1) and Cg(2) are centroid of atoms C1/C6 and C10/C15, intramolecular hydrogen bonding and π-π distances for (**I**) are represented in Table 3 (Figure 3).

**Table 3.** *The geometric details of the intra-/inter-molecular interactions (Å, °)*

| D-H⋯A | D-H | H⋯A | D⋯A | D-H⋯A |
|---|---|---|---|---|
| O1-H1⋯N1 | 0.82(4) | 1.82(4) | 2.565(3) | 150(3) |
| C7-H7A⋯O1$^i$ | 0.96 | 2.58 | 3.174(4) | 120 |
| C7-H7B⋯Cl2$^{ii}$ | 0.96 | 2.91 | 3.849(4) | 166 |
| C7-H7B⋯Cl2$^{iii}$ | 0.96 | 2.92 | 3.525(4) | 122 |

*Symmetry codes: (i) -x+1,+y,-z+1/2; (ii) -x+1,-y+1,-z +1; (iii) –x+1,-y,-z+1.*
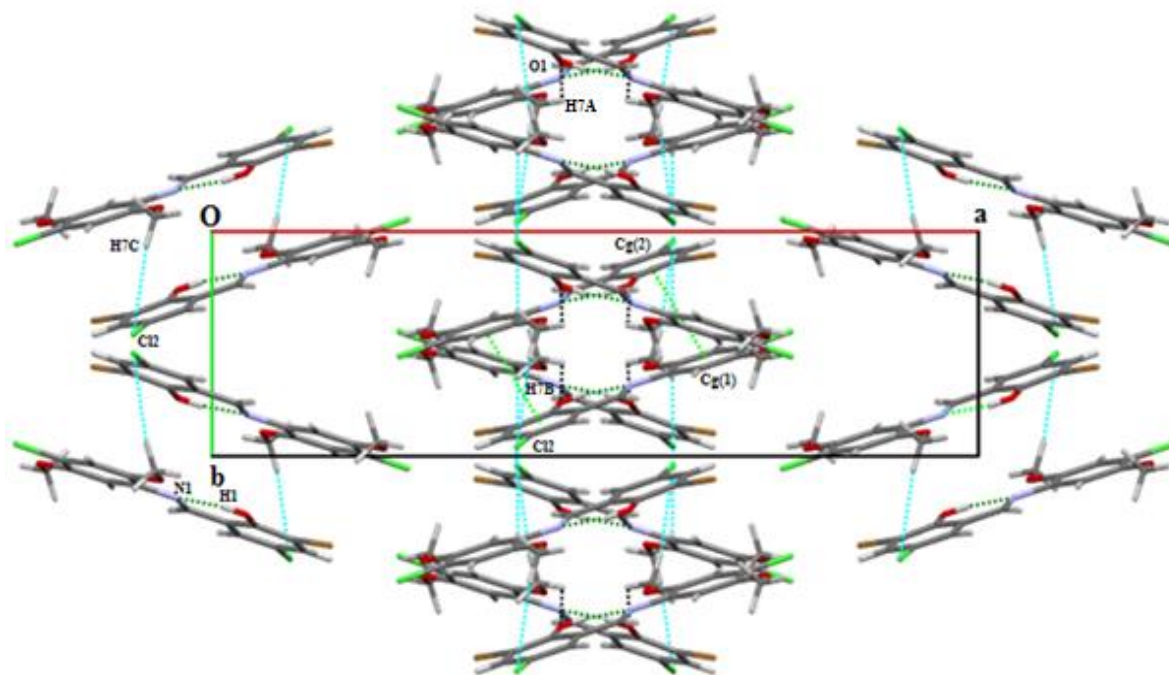


**Figure 3**. *Packing of the molecules when viewed along the c axis*

### 3.2. Optimized Geometry

Comparison of selected bond lengths and angles obtained by the X-ray and DFT (Figure 4) methods of (**I**) are listed in Table 2. The geometrical parameter values calculated of (**I**) are consistent with those obtained by X-ray structure determination within the error limits. Very small differences between the theoretical and experimental results are observed due to the theoretical calculations are performed in gas phase. As we discussed in crystallographic section, dihedral angle between two phenyl rings of the molecule is found as $2.28(8)^{o}$. But this angle is calculated as $28.10^{o}$. It can explain this difference that the single-crystal X-ray diffraction result belongs to solid state of (**I**), while the theoretical result is related to the gas phase of the isolated molecule. The most important bond parameters are C-N and C-O bond lengths for the Schiff-bases. C9-N1 and C15-O1 bond lengths of (**I**) are observed as 1.275(3) Å, 1.331(3) Å and calculated as 1.2754 Å, 1.3305 Å, respectively. The molecule adopts *E*-configuration in connection with C1=N1 double bond with C1-N1-C9-C10 torsion angle. This torsion angle of (**I**) is experimentally found as $178.9(2)^{o}$ and this torsion angle is calculated as $178.9150^{o}$ with DFT method.
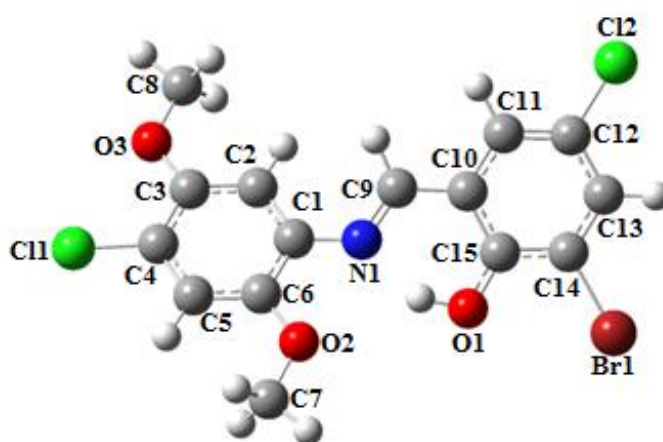


***Figure 4.*** *DFT geometry optimization of (**I**)*

In addition, we perform a global comparison by superimposing the molecular skeletons which are obtained from X-ray diffraction and the theoretical calculations by atom (Figure 5), obtaining RMSE's values of 0.419 Å for DFT/B3LYP method with the 6-311G(d,p) basis set. We can explain this magnitude of RMSE by using the fact that the neighboring molecules do not experience intermolecular coulombic interactions in gas phase, whereas the experimental results lead us to an interacting molecule in the crystal lattice.
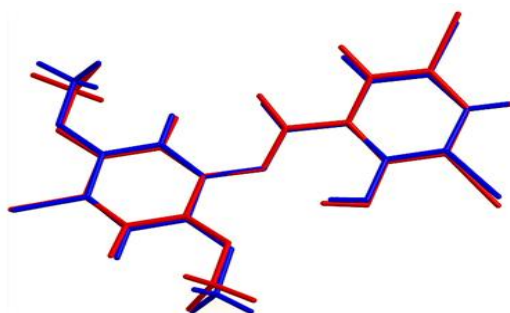


***Figure 5.*** *Superposition of the molecular structure obtained from the X-ray diffraction experiment (blue) and DFT calculation (red)*

### 3.3. Non-Linear Optic (NLO)

Theoretical investigations have been done in order to understand the microscopic origin of non-linear optical behavior of the studied molecule. The DFT has been used to calculate the $\mu$, $\alpha$ and $\beta_{total}$ and $\beta_{vec}$ for (**I**) in terms of $x$, $y$, $z$ components and are given by following equations [24]:

$$\mu = \sqrt{\mu_x^2 + \mu_y^2 + \mu_z^2} \tag{1}$$

$$\alpha = \frac{\alpha_{xx} + \alpha_{yy} + \alpha_{zz}}{3} \tag{2}$$

$$\beta = \sqrt{(\beta_{xxx} + \beta_{xyy} + \beta_{xzz})^2 + (\beta_{yyy} + \beta_{xxy} + \beta_{yzz})^2 + (\beta_{zzz} + \beta_{xxz} + \beta_{yyz})^2} \tag{3}$$

$$\beta_{vec} = \frac{3}{5}\left[\left(\beta_x^2 + \beta_y^2 + \beta_z^2\right)^{1/2}\right] \tag{4}$$

The polarizability and hyperpolarizability tensors ($\alpha_{xx}$, $\alpha_{xy}$, $\alpha_{yy}$, $\alpha_{xz}$, $\alpha_{yz}$, $\alpha_{zz}$ and $\beta_{xxx}$, $\beta_{xxy}$, $\beta_{xyy}$, $\beta_{yyy}$, $\beta_{xxz}$, $\beta_{xyz}$, $\beta_{yzz}$, $\beta_{xzz}$, $\beta_{yzz}$, $\beta_{zzz}$) can be obtained by a frequency job output file of Gaussian. However, $\alpha$ and $\beta$ values of Gaussian output are in atomic units (a.u.) so they have been converted into electrostatic units (esu) ($\alpha$: 1 a.u.=0.1482x10$^{-24}$ esu, $\beta$: 1 a.u.=8.6393x10$^{-33}$ esu). The $\mu$, $\alpha$ and $\beta$ have been calculated for (**I**) using B3LYP method of DFT with 6-311G(d,p) basis set. Calculated $\mu$, $\alpha$ and $\beta$ are 2.6339 D, 34.2373 Å$^3$ and 29.1857x10$^{-30}$ cm$^5$/esu, respectively (Table 4). Urea is the reference molecule which is used in the study of the NLO properties of molecular systems. Therefore, it is used commonly as a threshold value for comparative purpose. Calculated $\beta_{total}$ value for the title molecule (29.1857x10$^{-30}$ cm$^5$/esu) is found to be 149.9 times greater than the $\beta_{total}$ value of urea (0.1947x10$^{-30}$ cm$^5$/esu), predicting that (**I**) is an efficacious candidate for NLO material.

**Table 4.** *Calculated μ, α and β, components, β$_{tot.}$ and β$_{vec}$ values in gas phase of (**I**)*

|  | DFT |  | DFT |
|---|---|---|---|
| $\mu_x$ | -0.9269 a.u. | $\beta_{xxx}$ | 3114.1133 a.u. |
| $\mu_y$ | 0.4424 a.u. | $\beta_{xxy}$ | 864.4278 a.u. |
| $\mu_z$ | 0.1382 a.u. | $\beta_{xyy}$ | 68.5652 a.u. |
| $\mu_{tot.}$ | **2.6339 Debye** | $\beta_{yyy}$ | 181.8993 a.u. |
|  |  | $\beta_{xxz}$ | -4.6033 a.u. |
| $\alpha_{xx}$ | 422.7538 a.u. | $\beta_{xyz}$ | 119.1113 a.u. |
| $\alpha_{xy}$ | 18.5312 a.u. | $\beta_{yyz}$ | 37.0982 a.u. |
| $\alpha_{yy}$ | 269.447 a.u. | $\beta_{xzz}$ | -13.3992 a.u. |
| $\alpha_{xz}$ | 2.5977 a.u. | $\beta_{yzz}$ | 17.4203 a.u. |
| $\alpha_{yz}$ | 0.9417 a.u. | $\beta_{zzz}$ | 4.7360 a.u. |
| $\alpha_{zz}$ | 108.3616 a.u. | $\beta_{tot.al}$ | **29.1857x10$^{-30}$cm$^5$/esu** |
| $\alpha_{total}$ | **34.2373 Å$^3$** | $\beta_{vec}$ | **17.5114x10$^{-30}$cm$^5$/esu** |

### 3.4. Energies and Dipol Moments

We carried our calculations in vacuo and in different organic solvents (benzene, chlorobenzene, ethanol, methanol and water) for the evaluation of energetic behavior of (**I**) in solvent media, The calculated total molecular energies, frontier orbital energies and dipole moments using the PCM by B3LYP/6-311G(d,p) are listed in Table 5. As shown in Table 5, we can conclude that the total molecular energies, the electronegativity ($\chi$) and the softness ($S$) obtained by PCM method decrease with increasing polarity of the solvent, while the dipole moments, an energy gap ($\Delta E$) and global hardness ($\eta$) will increase more than the increase of the polarity of the solvent. According to these results, the stability of compound (**I**) increases in going from the gas to the solvent phase.

**Table 5.** *The calculated HOMO, LUMO, energy values, ΔE, I, A, χ, η, S and μ of (I) for five different solutions*

|  | DFT/B3LYP with 6-311G(d,p) | | |
|---|---|---|---|
|  | Gas phase ($\varepsilon = 1$) | Benzene ($\varepsilon = 2.3$) | Chlorobenzene ($\varepsilon = 5.62$) |
| $E_{total}$ (Hartree) | -4354.0237786 | -4354.0291402 | -4354.0331044 |
| $E_{HOMO}$ (eV) | -5.915 | -5.877 | -5.868 |
| $E_{LUMO}$ (eV) | -2.431 | -2.403 | -2.389 |
| $\Delta E$ (eV) | 3.484 | 3.474 | 3.479 |
| $I = -E_{HOMO}$ (eV) | 5.915 | 5.877 | 5.868 |
| $A = -E_{LUMO}$ (eV) | 2.431 | 2.403 | 2.389 |
| $\eta = (I-A)/2$ (eV) | 1.7420 | 1.7370 | 1.7395 |
| $\chi = (I+A)/2$ (eV) | 4.173 | 4.140 | 4.129 |
| $S = 1/2\eta$ (eV)$^{-1}$ | 0.28703 | 0.28785 | 0.28744 |
| $\mu$ (D) | 2.6339 | 2.8889 | 3.0881 |

|  | Ethanol ($\varepsilon = 24.55$) | Methanol ($\varepsilon = 32.7$) | Water ($\varepsilon = 78.35$) |
|---|---|---|---|
| $E_{total}$ (Hartree) | -4354.0358194 | -4354.0360371 | -4354.0364547 |
| $E_{HOMO}$ (eV) | -5.869 | -5.870 | -5.870 |
| $E_{LUMO}$ (eV) | -2.381 | -2.380 | -2.379 |
| $\Delta E$ (eV) | 3.488 | 3.490 | 3.491 |
| $I = -E_{HOMO}$ (eV) | 5.869 | 5.870 | 5.870 |
| $A = -E_{LUMO}$ (eV) | 2.381 | 2.380 | 2.379 |
| $\eta = (I-A)/2$ (eV) | 1.7440 | 1.745 | 1.7455 |
| $\chi = (I+A)/2$ (eV) | 4.125 | 4.125 | 3.491 |
| $S = 1/2\eta$ (eV)$^{-1}$ | 0.28670 | 0.28653 | 0.28645 |
| $\mu$ (D) | 3.2510 | 3.2654 | 3.2937 |

### 3.5. Mulliken Population Analysis (MPA)

The calculations of Mulliken atomic charges play an important role in the application of quantum-mechanical calculations to molecular systems [25]. The Mulliken atomic charges for (**I**) in gas phase are calculated at the B3LYP/6-311G(d,p) level. These charges are exhibited in Table 6. As can be seen in results that all the hydrogen atoms have a net positive charge, the obtained atomic charge shows that the H1 atom has bigger positive atomic charge (0.2772e) than the other hydrogen atoms. Furthermore, results from Table 6 show that N1 and O1 have higher negative value than the other atoms. This is due to the presence of O1-H1···N1 strong intramolecular hydrogen bond. Relativite to other atoms in the molecule; O1, O2, O3 and N1 atoms are most negative atomic charges (-0.3406e, -0.3389e, -0.3394e and -0.4730e, respectively). Moreover, Mulliken atomic charges also showed that C4, C12 and C14 atoms bonded Cl1, Cl2 and Br1 atoms, separately, has bigger negative atomic charges (-0.2779e, -0.2629e and -0.2185e, respectively) because of the steric effects.

**Table 6.** *Mulliken atomic charges of (I)*

| Atom | Mulliken charges | Atom | Mulliken charges | Atom | Mulliken charges |
|------|------------------|------|------------------|------|------------------|
| Br1 | 0.0045 | C6 | 0.1996 | H5 | 0.1274 |
| Cl1 | -0.0584 | C7 | -0.1377 | H7A | 0.1376 |
| Cl2 | -0.0403 | C8 | -0.1386 | H7B | 0.1107 |
| **O1** | **-0.3406** | C9 | 0.2397 | H7C | 0.1178 |
| **O2** | **-0.3389** | C10 | -0.2138 | H8A | 0.1419 |
| **O3** | **-0.3394** | C11 | 0.0662 | H8B | 0.1168 |
| **N1** | **-0.4730** | **C12** | **-0.2629** | H8C | 0.1116 |
| C1 | 0.1069 | C13 | 0.1141 | H9 | 0.0971 |
| C2 | -0.1064 | **C14** | **-0.2185** | H11 | 0.1170 |
| C3 | 0.3071 | C15 | 0.3099 | H13 | 0.1342 |
| **C4** | **-0.2779** | **H1** | **0.2772** | | |
| C5 | -0.0096 | H2 | 0.1187 | | |

### 3.6. Frontier Molecular Orbitals (FMOs)

The FMOs are frequently used to make a survey of the reactions between the compounds or electronic spectrum of (**I**). Because their energies define the capability of electron giving and accepting. Representation of the FMOs is given in Figure 6. We see that HOMO electrons are delocalized on C10 and C11 atoms while the LUMO electrons are only delocalized on N1 and C9 atoms. The energy difference between FMOs were related to global hardness and softness of (**I**).



$E_{HOMO} = -5.915$ eV

$\Delta E = 3.484$ eV

$E_{LUMO} = -2.431$ eV
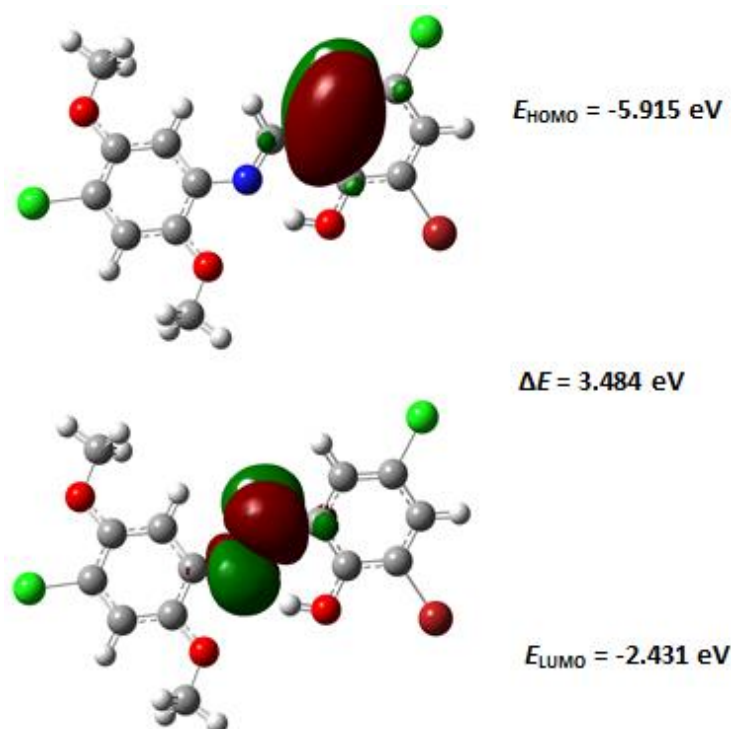
*Figure 6. The molecular orbital surfaces and energies for the HOMO and LUMO for (**I**)*

Total energies, dipole moments, energies of FMOs and the energy gap between the FMOs were calculated in vacuum and the different solvents, as mentioned in section energies and dipole moments for (**I**). The summarized results are given in Table 5. As a result of increasing solvent polarity, the FMOs gap increases while the total energy of the molecule decreases. On the other hand, the increasing the dipole moment of the molecule increases solvent polarity.

### 3.7. Molecular Electrostatic Potential (MEP)

The MEP is a helpful descriptor to visualize the electrophilic or nucleophilic reactive sites of molecules, and to show the electrostatic potential regions in terms of colour grading. The 3D plots of the MEP of the title compound are illustrated in Figure 7. In MEP map, different colours are represented by different values of the electrostatic potential: green represents the region of zero potential whereas red and blue represent the regions of the most negative and positive electrostatic potential. Potential increases by order: red < orange < yellow < green < blue. The colour code of this map ranges from    -0.0459 a.u. and +0.0459 a.u., where blue indicates the strongest attraction and yellow indicates repulsion. The positive regions are placed around all hydrogen atoms, which are related to nucleophilic reactivity [26]. The negative regions are located around the oxygen atoms (O1, O2 and O3; -0.0447, -0.0229 and -0.0284a.u., respectively). As shown in Figure 7, the positive potential sites are hydrogen and carbon atoms and the negative potential sites are around the electronegative atoms, while the remaining species are surrounded by orange, yellow and green. As we conclude from this, our title molecule is ready for both electrophilic and nucleophilic reactions.
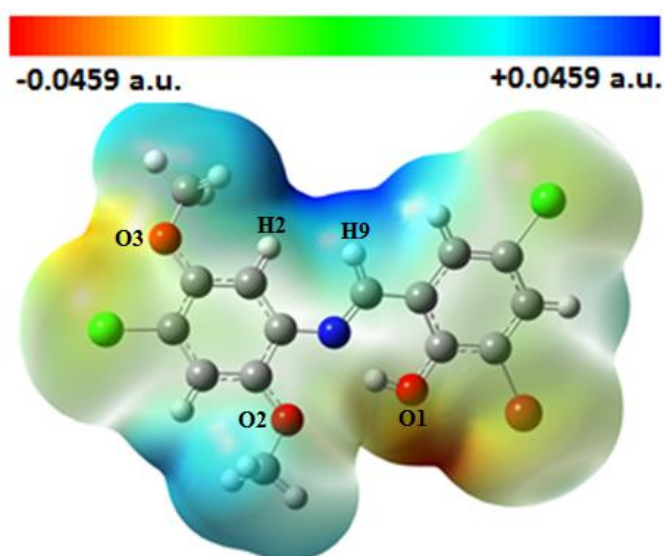


*Figure 7. MEP diagram of (**I**)*

### 3.8. Thermodynamic Properties

The standard thermodynamic functions of heat capacity ($C_v$), entropy ($S$), and enthalpy ($H$) changes for (**I**) were obtained from the theoretical harmonic frequencies, assuming vibrationally analysis and statistical thermodynamics, and these results are listed in Table 7. These thermodynamic functions increase as the temperature increases between 100 and 800 K due to the increase in temperature and molecular vibration intensity, as observed in Table 7. The correlation equations between heat capacity, entropy, enthalpy changes and temperatures were fitted by quadratic formulae, and the corresponding fitting factors ($R^2$) for these thermodynamical properties are 0.99998, 0.99977 and 0.99976, respectively. The corresponding fit equations are given as follows; the correlation graphs are shown in Figure 8.

$$C_V = 8.68776 + 0.26834 \text{ T} - 1.25785 \times 10^{-4} \text{ T}^2 \tag{5}$$

$$S = 66.45158 + 0.33501 \text{ T} - 1.0425 \times 10^{-4} \text{ T}^2 \tag{6}$$

$$H = -2.25016 + 0.03236 \text{ T} + 7.74773 \times 10^{-4} \text{ T}^2 \tag{7}$$

These data helped to provide information for further study on (**I**) in order to calculate the other thermodynamical energies according to the relationships between thermodynamical functions and to estimate the directions of the chemical reactions according to the second law of thermodynamics.
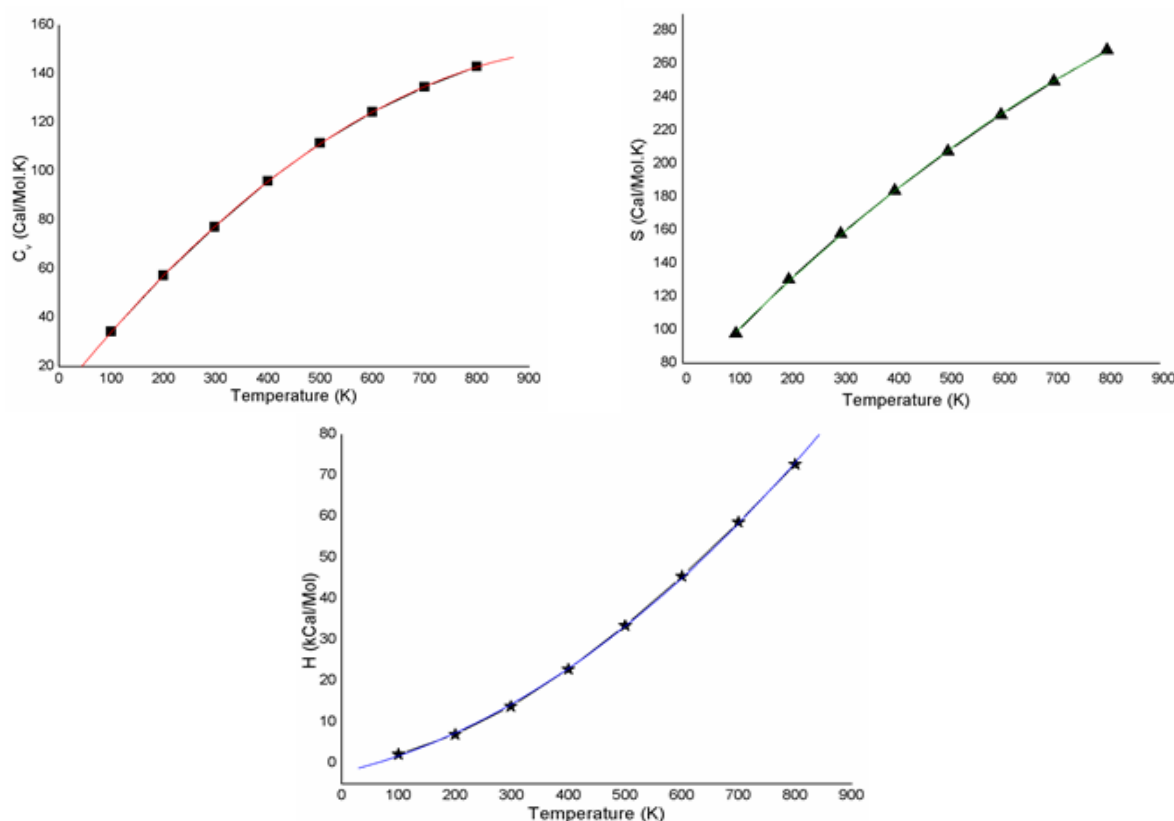
*Figure 8. Correlation graphics of thermodynamic properties and temperatures for (**I**)*

*Table 7. Thermodynamic properties at different temperatures at the B3LYP/6-311G(d,p) level for (**I**)*

| Temperature (K) | $C_v$ (Cal/Mol.K) | $S$(Cal/Mol.K) | $H$ (kCal/Mol) |
|---|---|---|---|
| 100 | 34.316 | 97.867 | 2.201 |
| 200 | 57.324 | 130.375 | 7.023 |
| 298.15 | 77.256 | 157.819 | 13.834 |
| 400 | 96.045 | 183.793 | 22.884 |
| 500 | 111.664 | 207.402 | 33.493 |
| 600 | 124.371 | 229.371 | 45.516 |
| 700 | 134.639 | 249.639 | 58.683 |
| 800 | 143.009 | 268.374 | 72.778 |

## 4. CONCLUSIONS

In present study, (*E*)-2-bromo-4-chloro-6-[(4-chloro-2,5-dimethoxyphenylimino)methyl]phenol, $C_{15}H_{12}BrCl_2NO_3$, (**I**), was prepared and investigated by a structural method. To support the experimental findings, the geometrical parameters of (**I**) have been calculated using the DFT method, and compared with the experimental data. It was noted here that the experimental results belong to solid phase, and theoretical calculations belong to gas phase. When the geometric parameters of (**I**) are compared against experimental data, it is seen that there are no significant differences. The value of the $\Delta E$ explains the eventual charge transfer interaction taking place within the molecule of compound. The total energy of the molecule decreases with the increasing polarity of the solvent for (**I**). The electronegativity ($\chi$) and the softness ($S$) obtained by PCM method decrease with increasing polarity of the solvent, while the dipole moments, the energy gap ($\Delta E$) and global hardness ($\eta$) will increase more than the increase of the polarity of the solvent for (**I**). The correlations between the statistical thermodynamics and temperature are also obtained. It is seen that the results of the thermodynamic parameters show that the parameters: heat

capacity, entropy and enthalpy increase with the increasing temperature owing to the intensities of the molecular vibrations which increase with increasing temperature. We can determine that the studied structure exhibits good NLO activity. The value of $\beta$ and $\mu$ suggest the possibility of technological NLO applications. In MPA, N1 and O1 have higher negative value more than the other atoms of (**I**). This is due to the presence of O1-H1···N1 strong intramolecular hydrogen bond. MPA and MEP can be used for interpreting and predicting the reactive behavior of a wide variety of chemical systems in both electrophilic and nucleophilic reactions. Thus, very complete characterizations of studied novel compound were given in the present paper. We hope that the research presented herein will be helpful for the design and synthesis new materials.

## ACKNOWLEDGEMENTS

## SUPPLEMENTARY MATERIAL

Crystallographic data for the structural analysis have been deposited with the Cambridge Crystallographic Data Centre, CCDC No. 1532550. Copies of this information may be obtained free of charge from the Director, CCDC, 12 Union Road, Cambridge CB2 1EZ, UK (fax: +44-1223-336033; e-mail: deposit@ccdc.cam.ac.uk or www: http://www.ccdc.cam.ac.uk).

## CONFLICTS OF INTEREST

No conflict of interest was declared by the authors.

## REFERENCES

[1]  Kajal, A., Bala, S., Kamboj, S., Sharma, N., Sainiet, V., "Schiff bases: A Versatile Pharmacophore", J. Catal., 2013:1-14, (2013).

[2]  Abu-Dief, A.M., Mohamed, I'M., "A review on versatile applications of transition metal complexes incorporating Schiff bases", Beni-Suef Univ. J. Appl. Sci., 4(2): 119-133, (2015).

[3]  Kostova, I., Saso, L., "Advances in research of Schiff-base metal complexes as potent antioxidants", Curr. Med. Chem., 20(36): 4609-4632, (2013).

[4]  Dhar D.N., Taploo, C.L., "Schiff bases and their applications", J. Sci. and Indust. Res., 41(8): 501-506, (1982).

[5]  Bruker (2013). APEX-II, SAINT and SADABS. Bruker AXS Inc., Madison, Wisconsin, USA.

[6]  Sheldrick, G.M., "A short history of *SHELXS*", Acta Crystallogr., A64(1): 112-122, (2008).

[7]  Sheldrick, G.M., "Crystal structure refinement with *SHELXL*", Acta Crystallogr., C71(1): 3-8, (2015).

[8]  Farrugia, L.J., "WinGX and ORTEP for Windows: an update", J. Appl. Crystallogr., 45, 849-854, (2012).

[9]  Mercury, Version 3.5.1; CCDC, available online via ccdc.cam.ac.uk/products/mercury.

[10] Gaussian 03, Revision B.01, Gaussian Inc., Wallingford CT, (2004).

[11] Frisch, A., Nielsen, A.B., Holder, A.J., Gaussview Users Manual, Gaussian Inc., Pittsburgh, (2007).

[12] Becke, A.D., "Density functional thermochemistry. III. The role of exact exchange", J. Chem. Phys., 98: 5648-5652, (1993).

[13] Becke, A.D., "Density-functional exchange-energy approximation with correct asymptotic behavior", Phys. Rev. A, 38(6): 3098-3100, (1988).

[14] Lee, C., Yang, W., Parr, R.G., "Development of the Colle-Salvetti correlation-energy formula into a functional of the electron density", Phys. Rev. B37: 785-789, (1988).

[15] Tomasi, J., Mennucci, B., Cammi, R., "Quantum-mechanical continuum solvation models", Chem. Rev. 105(8): 2999-3093, (2005).

[16] Tanak, H., Toğurman, F., Kalecik, S., Dege, N., Yavuz, M., "2-{(*E*)-[(2-Methyl-3-nitrophenyl)imino]methyl}-4-nitrophenol", Acta Cryst. E69, 1085, (2013).

[17] Özdemir, N., Kağıt, R., Dayan, O., "Investigation of enol-imine/keto-amine tautomerism in (*E*)-4-[(2-Hydroxybenzylidene)amino]phenyl benzenesulphonate by experimental and molecular modelling methods", Mol. Phys., 114(6): 757-768 (2016).

[18] Koşar, B., Özek, A., Albayrak, Ç., Büyükgüngör, O., "(*E*)-4-Methoxy-2-(*p*-tolylimino-methyl)phenol", Acta Crystallogr., E66(2): 469, (2010).

[19] Koşar, B., Albayrak, Ç., Ersanlı, C.C., Odabaşoğlu, M., Büyükgüngör, O., "Molecular structure, spectroscopic investigations, second-order nonlinear optical properties and intramolecular proton transfer of (*E*)-5-(diethylamino)-2-[(4-propylphenylimino)methyl]phenol: A combined experimental and theoretical study", Spectrochimica Acta A(93): 1-9, (2012).

[20] Ersanlı, C.C., Albayrak, Ç., Odabaşoğlu, M., Erdönmez, A., "4-(2-Hydroxyphenyliminomethyle-ne)phenol", Acta Crystallogr., E60: 389-391, (2004a).

[21] Ersanlı, C.C., Odabaşoğlu, M., Albayrak, Ç., Erdönmez, A., "[2-(Hydroxymethyl)phenylimino-methyl]phenol", Acta Crystallogr., E60: 264-266, (2004b).

[22] Gökçe, H., Öztürk, N., Kazıcı, M., Yörür Göreci, Ç., Güneş, S., "Structural, spectroscopic, electronic, nonlinear optical and thermodynamic properties of a synthesized Schiff base compound: A combined experimental and theoretical approach", J. Mol. Struct., 1136: 288-302, (2017).

[23] Moustakali-Mavridis, I., Hadjoudis, E., Mavridis, A., "Crystal and molecular structure of some thermochromic Schiff bases", Acta Crystallogr. Sect. B34: 3709-3715, (1978).

[24] Zhang, R., Du, B., Sun, G., Sun, Y.X., "Experimental and theoretical studies on *o*-, *m*- and *p*-chlorobenzylideneaminoantipyrines", Spectrochim. Acta A, 75: 1115-1124, (2010).

[25] Mulliken, R.S., "Electronic population analysis on LCAO [Single Bond] MO molecular wave functions I.", J. Chem. Phys., 23(10): 1833-1840, (1955).

[26] Luque, F.J., López, J.M., Orozco, M., "Electrostatic interactions of a solute with a continuum. A direct utilization of ab initio molecular potentials for the prevision of solvent effects", Theoret. Chem. Accounts, 103: 343-345, (2000).